Original Article

Nano-graphene oxide/polyurethane nanofibers: mechanically flexible and myogenic stimulating matrix for skeletal tissue engineering

Seung Bin Jo[1,*] (iD), Uyanga Erdenebileg[1,2,*], Khandmaa Dashnyam[1,2,3], Guang-Zhen Jin[1,2,3], Jae-Ryung Cha[2], Ahmed El-Fiqi[1], Jonathan C. Knowles[2,3,4,5], Kapil Dev Patel[1,2,3], Hae-Hyoung Lee[1,3,6], Jung-Hwan Lee[1,2,3,6] and Hae-Won Kim[1,2,3,6] (iD)

Abstract

For skeletal muscle engineering, scaffolds that can stimulate myogenic differentiation of cells while possessing suitable mechanical properties (e.g. flexibility) are required. In particular, the elastic property of scaffolds is of importance which helps to resist and support the dynamic conditions of muscle tissue environment. Here, we developed highly flexible nanocomposite nanofibrous scaffolds made of polycarbonate diol and isosorbide-based polyurethane and hydrophilic nano-graphene oxide added at concentrations up to 8%. The nano-graphene oxide incorporation increased the hydrophilicity, elasticity, and stress relaxation capacity of the polyurethane-derived nanofibrous scaffolds. When cultured with C2C12 cells, the polyurethane–nano-graphene oxide nanofibers enhanced the initial adhesion and spreading of cells and further the proliferation. Furthermore, the polyurethane–nano-graphene oxide scaffolds significantly up-regulated the myogenic mRNA levels and myosin heavy chain expression. Of note, the cells on the flexible polyurethane–nano-graphene oxide nanofibrous scaffolds could be mechanically stretched to experience dynamic tensional force. Under the dynamic force condition, the cells expressed significantly higher myogenic differentiation markers at both gene and protein levels and exhibited more aligned myotubular formation. The currently developed polyurethane–nano-graphene oxide nanofibrous scaffolds, due to their nanofibrous morphology and high mechanical flexibility, along with the stimulating capacity for myogenic differentiation, are considered to be a potential matrix for future skeletal muscle engineering.

Keywords

Myogenic differentiation, nanofiber, mechanical stretch, graphene oxide, polyurethane

Date received: 17 September 2019; accepted: 18 December 2019

[1]Institute of Tissue Regeneration Engineering (ITREN), Dankook University, Cheonan, Republic of Korea
[2]Department of Nanobiomedical Science and BK21 PLUS NBM Global Research Center for Regenerative Medicine, Dankook University, Cheonan, Republic of Korea
[3]UCL Eastman-Korea Dental Medicine Innovation Centre, Dankook University, Cheonan, Republic of Korea
[4]Division of Biomaterials and Tissue Engineering, Eastman Dental Institute, University College London, London, UK
[5]The Discoveries Centre for Regenerative and Precision Medicine, Eastman Dental Institute, University College London, London, UK

[6]Department of Biomaterials Science, College of Dentistry, Dankook University, Cheonan, Republic of Korea

*Contributed equally to this paper as first authors.

Corresponding authors:
Jung-Hwan Lee, Institute of Tissue Regeneration Engineering (ITREN), Dankook University, Dandaero 119, Cheonan 31116, Republic of Korea.
Email: ducious@gmail.com

Hae-Won Kim, Institute of Tissue Regeneration Engineering (ITREN), Dankook University, Dandaero 119, Cheonan 31116, Republic of Korea.
Email: kimhw@dku.edu

Introduction

In both native and engineered tissues, communication between cells and extracellular matrix (ECM) is critical for appropriate tissue function.[1] In native human tissues, notably for soft tissues, like cardiac muscles and skeletal muscles, they have highly elastic properties. The elasticity of a biomaterial can be closely related to its biocompatibility when applied to elastic tissues such as muscles and tendons.[2] Therefore, tissue engineering of these soft tissues is closely related to the development of elastic biomaterials that can endure multiple strain cycles in harmony with the surrounding tissue.[3] Synthetic biodegradable elastomers usually have several unique features, including three-dimensional cross-linked networks, simulating the structure of naturally occurring elastic materials, biodegradability, physicochemical and mechanical properties such as stress relaxation, which is one of the important characteristics of soft tissues like muscle and tendon.[4] Therefore, these elastomers have attracted significant attention in the area of soft tissue regeneration because of their capacity to reproduce the mechanical properties of the supporting matrix.[5]

Many studies focus on the development of elastomeric biomaterials because it is important for biomaterials to mimic the biological and mechanical characters of native ECM.[6] Various biomaterials are designed to mimic several properties of ECM. For example, electrospun nanofibrous scaffold biomaterials have attracted significant interest in the field of tissue engineering, by reason of their large surface area and analogous physical structures to natural ECMs,[7,8] which has fibrous geometry.[9] Indeed, all living organisms are inseparable from the molecular behavior at the nanometer length scale, and ECM has a complex hierarchical 3D structure from the nano- to the centimeter scale.[10] Therefore, a number of researchers are interested in nanoscale biomaterials.[11–14] It seems that mechanical properties of electrospun nanofibrous scaffolds meet the requirements for applying in biological systems. Recent publications have shown an improvement in cell behavior and skeletal myofiber formation on the electrospun fiber sheath enhanced with topographical or electric cues in vitro.[15,16]

A number of studies have been conducted to apply natural and synthetic elastomers to a field of tissue repair and regeneration.[17] Among them, polyurethanes (PUs) are one of the widely studied synthetic elastic polymers in tissue engineering applications because of their biodegradability, mechanical flexibility, biocompatibility, and diverse compositions.[2,18] PU can be widely applicable because there are diverse selections of monomeric materials from various types of macrodiols, diisocyanates, and chain extender[19] that can be used for their synthesis. Furthermore, desired physicochemical properties can be easily introduced to synthesized PU by changing starting materials for the soft and hard segments as well as chain extenders.[20] Even though the physicochemical properties of PU can be altered to some extent, its low hydrophilicity, which is closely related to biocompatibility, has been of concern and a focus for researchers to improve via several routes.[21]

Polymer composites can show improved properties compared with polymers alone. The addition of biocompatible additives, such as hydroxyapatite (HA),[22] chitosan,[23] and carbon nanotubes (CNTs),[24] has been widely studied as various scaffolds to modify the mechanical performance, hydrophilicity, and interactions between cells and scaffolds. Graphene and its derivatives have attracted considerable attention in recent years in the field of biomaterials because of their unique physicochemical properties.[25,26] Graphene oxide (GO), one of the most important derivatives of graphene, has a large number of hydroxyl groups on its surface, with which GO is invested with hydrophilicity.[26] Although GO has been used for delivery systems[27,28] and cell culture systems,[29,30] the understanding of its cytotoxicity is still under debate. Some specific studies have found that the cytotoxicity of graphene and GO depends on the aggregation of GO and cell types,[31] applied dose, and time.[32,33] In addition, it seems that a low content of GO is nontoxic, while high dose and size of GO can cause oxidative stress in cells and induce loss of cell viability.[34]

Collectively, we considered the PU polymer nanocomposites with appropriate levels of nano-graphene oxide (nGO) might show not only improved mechanical properties such as tensile strength and hydrophilicity but also improved biocompatibility with minimal cell toxicity. In this study, we developed electrospun PU-nGO nanofibers and identified the mechanical properties that are suitable for skeletal muscle engineering. Also, we examined the initial adhesion and spreading of C2C12 cells and the subsequent myogenic differentiation when cultured on the nanofibrous scaffolds. Finally, we took advantage of the elastic property of the PU-nGO nanofibers by culturing under dynamic tensional conditions to synergize the scaffold properties with applied forces to address the possibility of the scaffolds for future skeletal muscle engineering.

Materials and methods

chemicals and reagents

Analytical grade chemical reagents were purchased from Sigma-Aldrich. The reagents include 2,2,2 trifluoroethanol (TFE, CF_3CH_2OH, ≥99%), chloroform ($CHCl_3$, 99.0%, Duksan chemicals, South Korea), (3-aminopropyl) triethoxysilane (APTES, $H_2N(CH_2)_3Si(OC_2H_5)_3$ ≥98%), N,N-dimethylformamide ((DMF), $HCON(CH_3)_2$, 99.8%), hexamethylene diisocyanate (HDI, $OCN(CH_2)_6NCO$), isopropyl alcohol (IPA, $(CH_3)_2CHOH$, 99.5%, Duksan chemicals, South Korea), dianhydro-D-glucitol (isosorbide, $C_6H_{10}O_4$, 98%), the aliphatic polycarbonate diol 2000

(PCD diol, T4672, Asahi Kasei chemical corporation). nGO powder was purchased from Calverton (NY, 11933, USA). The diameter of the nGO was around 90–200 nm, with about 1 nm thickness. The single-layer ratio was >99%, the purity of the particle was also >99%.

Preparation of PU

PU was incorporated by one-shot bulk polymerization from PCD diol and isosorbide. PCD diol (23.78 g, 11.89 mmol) and isosorbide (6.95 g, 47.57 mmol) were placed in a four-necked round-bottomed flask (250 mL) with a mechanical stirrer, thermometer, and condenser. The mixture of two diols was stirred under N_2 at 60°C for 1 h. HDI (10 g, 59.46 mmol) was combined to the mixture and they reacted at 120°C for 12 h. The synthesized PU was dispersed in DMF and precipitated in IPA (4 L). The precipitated PU was cleaned with IPA and vacuum-dried at 60°C for 24 h to prepare high-purity PU.

Preparation of fiber scaffolds

The PU was dissolved in chloroform by 10 wt.%. Meanwhile, 0%, 1%, 2%, 4%, and 8% nGO (calculated based on the dissolved PU) was dissolved in TFE and underwent ultrasonication for 5 min at 80°C for even dispersion. APTES was then added to each solution and also ultrasonicated for another 5°min. Each solution was mixed to be homogenized with stirring at room temperature.

Then, the mixed 10-mL solution was inserted into a 10-mL plastic syringe with a 23-gauge needle tip, placed on an injection pump of an electrospinning device. The injection rate of the electrospinning device was set at 2 mL/h with 12.5 kV and needle tip was fixed in 10 cm distance from the collecting drum. The drum was set by 500 r/min and collected the fiber on aluminum-foil sheet. Consequently, the obtained electrospun nanofibrous sheet was placed in an air hood to evaporate organic solvents.

Characterization of fiber scaffolds

The fiber was observed by a high-resolution scanning electron microscope (SEM, JEOL, Japan). Prior to observation, the fiber sheet was completely covered with platinum by an automatic magnetron sputter coater (Cressington 108 Auto sputter coater, UK) for 80 s. PU-nGO fibers were also observed by a high-resolution transmission electron microscope (HR-TEM, JEM-3-1-, JEOL, Japan). The effect of APTES on nGO particles was observed by x-ray diffraction (XRD, Rigaku, Ultima IV, Japan) using CuKα radiation (λ = 1.5418 Å). Electrospun fibers were also analyzed by Fourier transform infrared spectroscopy (FT-IR)

with the GladiATR diamond crystal component (PIKE Technologies, USA).

The electrical conductivity of the PU-nGO electrospun composite nanofibers was determined by a four-probe method using a Keithley 6514 electrometer, under wet condition. The experiment was performed at room temperature and resistivity of the samples were analyzed by following equation,

$$\rho = wRt / d$$

where, R = V/I is resistance, V = voltage, I electric current, w = width of nanofibers, t = thickness of the film, and d = distance between two probes. The reciprocal of obtained resistivity is the conductivity of the nanofibers. Five samples were analyzed for each condition.

The hydrophilicity of the fiber was determined via water contact angle (WCA) measurement, by the sessile drop method applying a benchtop phoenix contact angle measurement system (PHX300, SEO, South Korea). The fibrous sheet was placed on the camera stage for further scanning and approximately 2 µL distilled water from the syringe pump was beaded onto the surface of the sample (n = 5). Each droplet on fibrous materials was measured 0.1, 5, 10 min, respectively, and automatically recorded every 15 s using a video camera system (CCD camera) and the surface contact angles were determined by XP software.

The thermogravimetric analysis(TGA) was carried out in an alumina crucible with 5 mg mass sample for each polymer, using the simultaneous Thermal Analysis Modulus, SDT Q600 (TA Instruments) controlled by Advantage for Q Series software. The experiment was carried out under N_2 atmosphere (flow of 100 mL/min) from 24 to 700°C at 10°C/min and heating rate.

Mechanical properties of fiber

Uniaxial tensile test and stress relaxation test were conducted with the Universal testing machine (Instron, Norwood, MA, USA) and the results were recorded on the crossed-loop PC software (Bluehill 2, Instron). The materials were cut into 40 x 10.0 mm rectangular shape with 0.04 mm thickness and then stretched at a speed of 10 mm/min until the sample broke (n = 6). Based on the software, the tensile mechanical values were converted to stress-strain curves from which the stress-time curve and maximum tensile stress were calculated. In the case of stress relaxation properties, tension loads were applied to each specimen (40 mm diameter x 10 mm height) at a constant strain of 100% with a deformation rate of 600 s (n = 6). The corresponding stress was recorded along with the time and the time for the initial stress of the material to relax to half its value during a stress relaxation (tau 1/2) was also determined.

Table 1. Primer sequences for the RT-PCR analysis.

Gene	Forward sequence	Reverse sequence
α-Actinin	5'-GGACTACACTGCCTTCTC-3'	5'-CAGCCTATACTTCAGCCTTTA-3'
Myogenin	5'-TGTCTGTCAGGCTGGGTGTG-3'	5'-TCGCTGGGCTGGGTGTTAG-3'
MyoD	5'-GGAGTGGCAGAAAGTTAAG-3'	5'-ACGGGTCATCATAGAAGTC-3'
GAPDH	5'-GTGTTCCTACCCCCAATGTG-3'	5'-TCCACCACCCTGTTGCTGTA-3'

GAPDH: glyceraldehyde 3-phosphate dehydrogenase; RT-PCR: reverse transcription polymerase chain reaction.

Cell toxicity, adhesion, spreading, and proliferation assay

We cultured C2C12 cells of passage 3 to 8 with Dulbecco's modified eagle medium (DMEM) supplemented with 10% fetal bovine serum (FBS; Gibco, USA), 1% Pen/Strep (Invitrogen, USA), at 37°C with 5% CO_2. For indirect cyto-toxicity test, an extract of each specimen is prepared with supplemented media ($6 cm^2$/mL) for 24 h at 37°C, and it was added to C2C12 cells in 96-well plates for 24 h (n = 5). Then a CCK-8 analysis was performed according to the manufacturer's protocol for determining cell viability. For cell adhesion and spreading assay, the electrospun specimens were prepared as 5 mm diameter round shaped membranes (n = 5). All membranes were incubated with 300 μL of medium in 37°C for 4 h. Cells were seeded on PU or PU-nGO fiber membranes each with 1.0×10^4 cells and these membranes were incubated for 2 or 4 h at 37°C. Cells were then fixed with 4% paraformaldehyde (PFA) solution at 4°C for 20 min, followed by phosphate-buffered saline (PBS) washing for three times, and then treated with 0.2% Triton X-100 (Sigma) for 10 min followed by 1% bovine serum albumin (BSA) for 30 min each. Mouse anti-Vinculin antibody (ab18058, Abcam) was diluted at 1:200 in 1% BSA and treated to cells at 4°C overnight. After being washed with PBS, cells were treated with fluorescein isothiocyanate (FITC)-conjugated secondary antibody (F0257, Sigma) for 2 h at room temperature. After washing with PBS, cells were counterstained by Alexa Flour 555 labeled (red) phalloidin (A34055, Invitrogen) and then with 4′,6-diamidino-2-phenylindole (DAPI; A12379, Invitrogen). Images of cells were taken by a confocal laser scanning microscope (CLSM; Zeiss LSM 700, Germany).

Cell proliferation was determined using Fluorescence Hoechst DNA Quantification Kit (Sigma). C2C12 cells were cultured on the electrospun specimens of 5 mm diameter with 96-well plate (SPL Life Sciences, Pocheon, Gyeonggi-do, Korea), 10,000 cells per each well for 24 h, and the specimens were harvested after 1, 3, and 5 days for proliferation assay (n = 5). In all, 200 μL of deionized water was added to the scaffolds at each time point followed by three freeze-thaw cycles to extract DNA from the scaffolds. A DNA standard curve was formulated by staining the DNA with Hoechst 33258 solution, using the DNA standards provided. The fluorescence was measured with excitation and emission wavelengths of 360 and 460 nm using a microplate reader (Bio-Rad, US).

Myogenic gene expression analysis

Real-time reverse transcription polymerase chain reaction (RT-PCR) was used to analyze the expression level of actinin, myogenin, and MyoD. The cDNA was directly synthesized from cultured cells using an iScript™ DNA synthesis kit (BioRad, US). Real-time RT-PCR using SensiMix™ SYBR® Hi-ROX Kit (Biokine, US) was performed with an AB 7500 Real-Time PCR System (Life Technologies, US). Thermocycling conditions were as follows: 95°C for 5 min, 40 cycles of denaturation (15 s, 90°C), annealing (15 s, 55°C), and extension (15 s, 72°C). The primer sequences are listed in Table 1. The housekeeping gene glyceraldehyde 3-phosphate dehydrogenase (GAPDH) was used to normalize the data using the 2 − ΔΔCt method (n = 4).

Myotube formation and immunocytochemistry

C2C12 were seeded at a density of 3×10^4 cells/well on materials with 48-well plate. After 1 day, the cells were incubated in differentiation media (DM; DMEM containing 2% horse serum and 1% Pen Strep (Invitrogen, Carlsbad, CA, USA)) for a further 3 days to induce myotube formation (n = 4). DM was changed every other day. In the case of dynamic culture, the specimens with cultured cells went through the same differentiation conditions under dynamic tension using Flexcell machine (Dunn Labortechnik, Asbach, Germany) with 10% strain, 0.5 Hz, and 0, 1, 4, or 16 h tension stimuli on each day (n = 4). On the third day of differentiation, the cells were fixed with 4% PFA, permeabilized with 0.2% Triton X-100, blocked with 1% BSA solution, incubated with primary antibody (MHC: 1:200, Santa Cruz) at 4°C overnight, incubated with secondary antibody (Dylight 488-conjugated goat anti-mouse IgG; 1:100; Abcam) at RT for 2 h, and mounted with Vectashield mounting solution. The multinucleate myotubes were observed using a fluorescence microscope.

Statistical analysis

All of the quantitative results were expressed as mean standard error of the mean (SEM). Statistical analysis was carried out by means of one-way analysis of variance (ANOVA). A p-value of less than 0.05 was considered statistically significant.

Results and discussion

Physicochemical properties of PU or PU-nGO nanofibers

XRD pattern of synthesized nGO particles from graphene showed a broad reflection at approximately 10°, but once APTES was added in nGO solution, a peak appeared at 20° (Figure 1(b), left panel). The FT-IR spectra of the nGO samples showed an intense OH peak represented at $3200\,cm^{-1}$, and a distinct C=O peak at $1600\,cm^{-1}$, which is related to carboxylic acid and carbonyl functional groups (Figure 1(b), right panel). The activated nGO particles were incorporated into the PU solution, and the PU or PU-nGO fibers were prepared by electrospinning (Figure 1(a)). The FT-IR spectra of PU or PU-nGO fibers showed that peaks of hydroxyl and ether groups were present at $1220\,cm^{-1}$(Figure 1(c)), and the peak intensity became stronger as the content of nGO increased. In addition, TGA analysis of nGO, pure PU fiber, and nGO-incorporated PU fiber were conducted (Supplementary Figure1). The nGO-incorporated PU showed two weight loss events, unlike pure PU which showed a single event, ensuring that nGO was well incorporated into PU fiber.

SEM images of the GO-embedded electrospun PU fiber showed the fiber surface morphology (Figure 1(d)). nGO particles were incorporated at various amounts (0 ~ 8 wt%) into PU solutions to fabricate electrospun fiber matrices. The fibers were easily produced with a smooth and relatively uniform surface when fabricated with 1%–8% nGO addition, as well as for pure PU fibers. TEM images of the PU-nGO samples were also taken to examine the internal nanostructure of the fibers. The PU-nGO fibers also showed smooth surface with no nGO aggregation in TEM images. TEM images showed slightly increased PU-nGO fiber size compared to pure PU fiber, but all the fiber diameters measured were less than 1 μm. The electroconductivity of the fibers was also measured (Figure 1(d)), as the incorporation of carbon-based materials may alter the electroconductive properties which also affects the muscle cell functions.[35] Under the wet conditions, only 8% PU-nGO fiber showed electroconductive behaviors. The PU-nGO fibers of 1%–4% addition showed unmeasurable electrical conductivity. Although the GO itself is known as a nonconducting material, the electroconductivity can be restored by its graphitic network in several ways.[26]

The poor wettability of polymeric scaffolds often limits the cellular interactions such as adhesion and subsequent differentiation.[13,36] The WCA of PU and PU-nGO nanofibers were recorded with time (Figure 1(e)). The incorporation of nGO significantly enhanced the wettability, 0% < 1% < 2 ~ 4% << 8%. The result was consistent with our FT-IR data, in relation to the hydroxyl and carboxyl functional groups of nGO (Figure 1(b) and (c)).

Mechanical characteristics of PU or PU-nGO nanofibers

The tensile strength and elastic modulus are of important mechanical characteristics and can be changed via modification of the composition, especially via nGO incorporation into nanofibrous matrices. The elastic modulus of PU-nGO nanofibers were greatly increased with nGO incorporation (Figure 2(a) and (c)), and their maximum tensile stress values were in the range of 12–20 MPa, which were similar to the pure PU fiber (Figure 2(b)). In addition, the proportional limits of nanofibers were around 40% to 60%, which revealed that the incorporation of nGO did not mitigate the flexibility of PU (Figure 2(d)). Stress relaxation, or energy dissipation, is one of the important characteristics of soft tissues like muscle and tendon.[4] Stress-relaxation experiments of PU-nGO nanofibers are conducted with 100% constant strain (Figure 2(e) and (f)). All specimens showed clear stress relaxation tendency (Figure 2(e)), and 4%–8% PU-nGO fiber showed the lowest tau 1/2 value (Figure 2(f)), suggesting that these PU-nGO fibers showed good stress-relaxation properties.

Cytocompatibility of C2C12 cells to PU or PU-nGO nanofibers

Several cell behaviors to PU or PU-nGO nanofibrous matrices were evaluated with the C2C12 cell line; an easily obtained and widely employed murine skeletal myoblast cell line. C2C12 myoblast cells were seeded on each fiber membrane and incubated to determine initial adhesion and spreading capacity (Figure 3(a)–(c)), as well as to identify proliferative and cytotoxic effects (Figure 3(d) and Supplementary Figure 2). Vinculin is known for being a physical link between ECM and the intracellular actin cytoskeleton and these vinculin and actin cytoskeletons are known to be crucially involved in cell adhesion and spreading.[37–39] After cells being seeded onto nanofibers and incubated for 4 h, initial attachment number and spreading area of C2C12 cells were identified with actin, vinculin, and DAPI staining. All the C2C12 cells exhibited normal spindle shapes, indicating the stable adhesion of cells to the substrate (Figure 3(c)). Compared to the PU nanofiber, all the PU-nGO nanofibers showed elevated cell adhesion capacity (Figure 3(a)). Furthermore, cell spreading areas were significantly improved along with the nGO incorporation: 0% < 1% ~ 2% < 4% ~ 8% (Figure 3(b)). These results are partially consistent with previous reports that GO enhances cell attachment,[40] that nGO promotes neurite sprouting and outgrowth,[41] and that the nanoscale substrate condition is critical for cell attachment and differentiation.[42] Consistently, the PU-nGO nanofibers showed no cytotoxic effect to C2C12 cells (Supplementary Figure 2), and cells were more proliferative as the nGO content increased, especially the 8% PU-nGO showing the
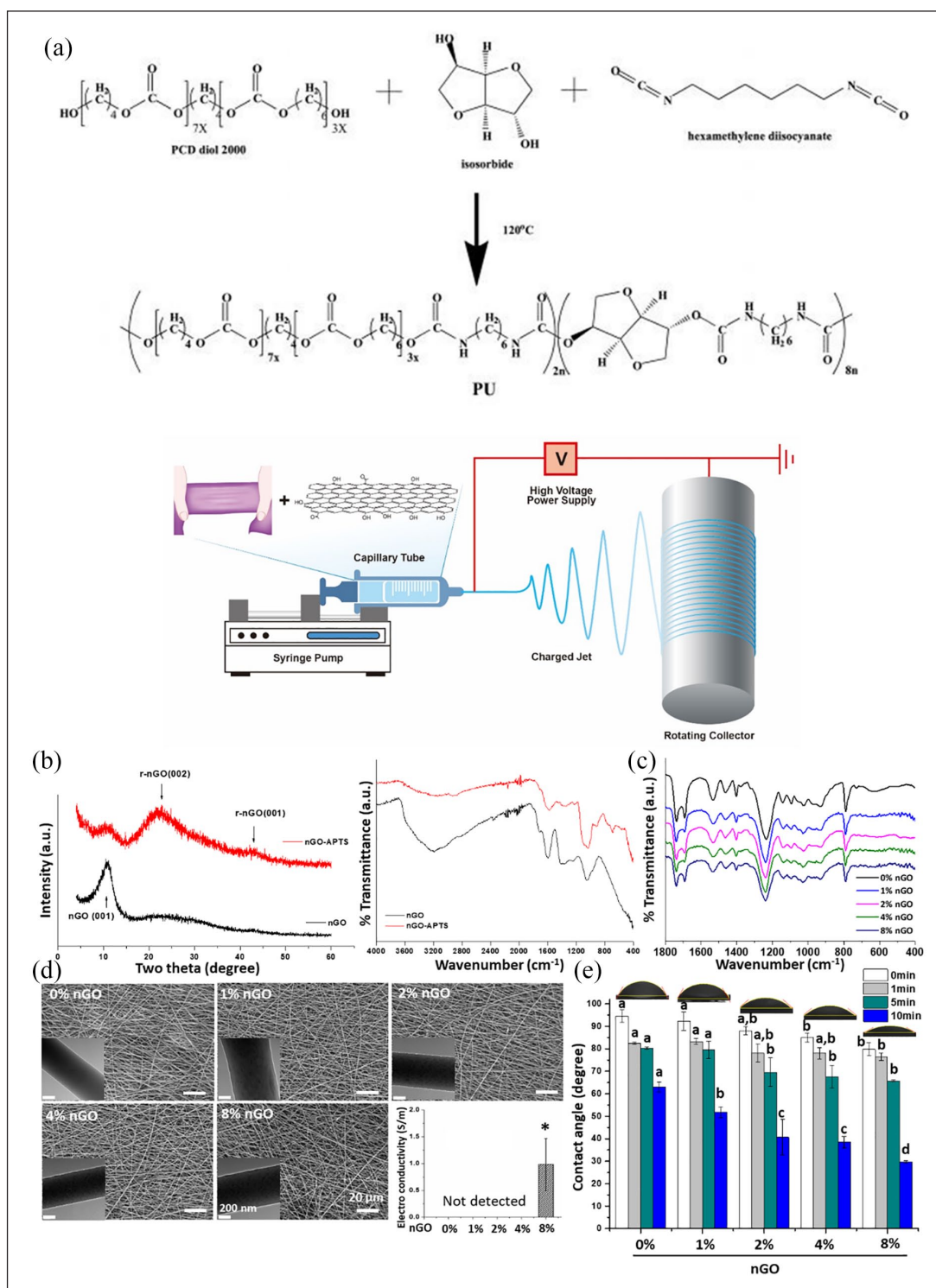
Figure 1. Preparation of PU-nGO nanofibers and the physicochemical characteristics. (a) Chemical structure of polyurethane (PU) after one-shot bulk polymerization from PCD diol and isosorbide, and conjugation nGO in PU to prepare nanofibrous scaffolds by electrospinning. (b) XRD and FTIR of nGO after APTES treatment for activating GO. When activated, the peak shifted from 10° to 20° (b, left panel), OH peak represented at $3200\,cm^{-1}$, and C=O peak at $1600\,cm^{-1}$ were changed (b, right panel), (c) FT-IR of nGO conjugated PU nanocomposite. Intense peak of $1220\,cm^{-1}$ represents the ester or hydroxyl group, and it became stronger along with nGO content. Each graph of FT-IR has been presented for easy comparison by giving an offset of 10% from top to bottom. (d) SEM and TEM images of PU-nGO fibers morphology and electroconductivity of fibers. The fibers were finely fabricated with no nGO aggregation. Under wet conditions, only 8% PU-nGO showed electroconductivity. (e) Water contact angle (WCA) analysis to determine hydrophilicity of fiber scaffolds by time 0–10 min. Fibers with more nGO showed higher hydrophilicity. An asterisk in (d) showing a statistically significant difference compared to 0% ($p < 0.05$, $n = 5$). Different letters in (e) indicating significant differences among them at the same incubation time condition ($p < 0.05$, $n = 5$).
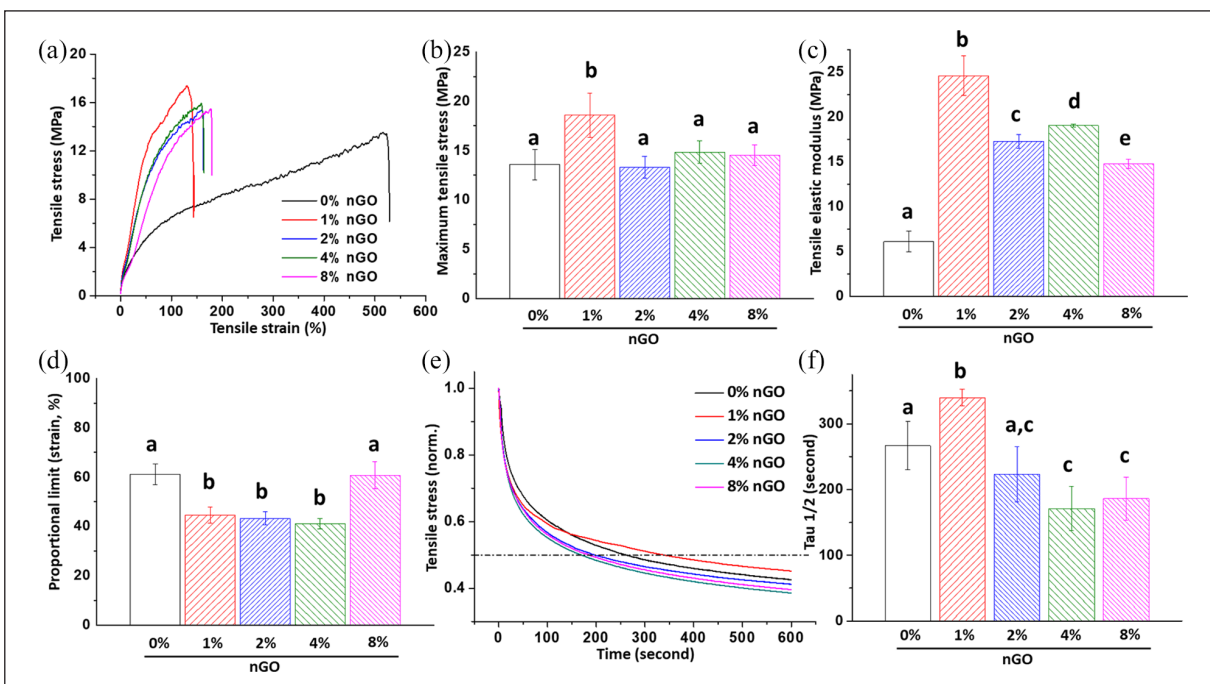
Figure 2. Mechanical characteristics of PU-nGO nanofiber. (a) Stress–strain curve of all PU-nGO nanofiberous membrane groups by Instron machine and analyzed data (b to d). (b) Maximum tensile stresses of nanofibers. They are in the range of 12–20 MPa. PU-nGO fibers preserved the flexibility of PU. (c) Tensile elastic modulus of nanofibers. All the PU-nGO nanofibers showed enhanced elastic modulus compared to pure PU. (d) Proportional limits of the nanofibers. They were in the range of 40%–60%. The 8% PU-nGO showed a similar level of the proportional limit of PU's one. (e, f) Stress relaxation at 100% strain. (e) Stress relaxation curve. All nanofibers showed stress relaxation tendencies. (f) Tau 1/2 of all the groups based on the stress relaxation curve. The 4% and 8% PU-nGO groups showed the shortest tau 1/2 value, representing the best stress-dissipation capacity. Different letters indicating significant differences among them ($p < 0.05$, $n = 6$).
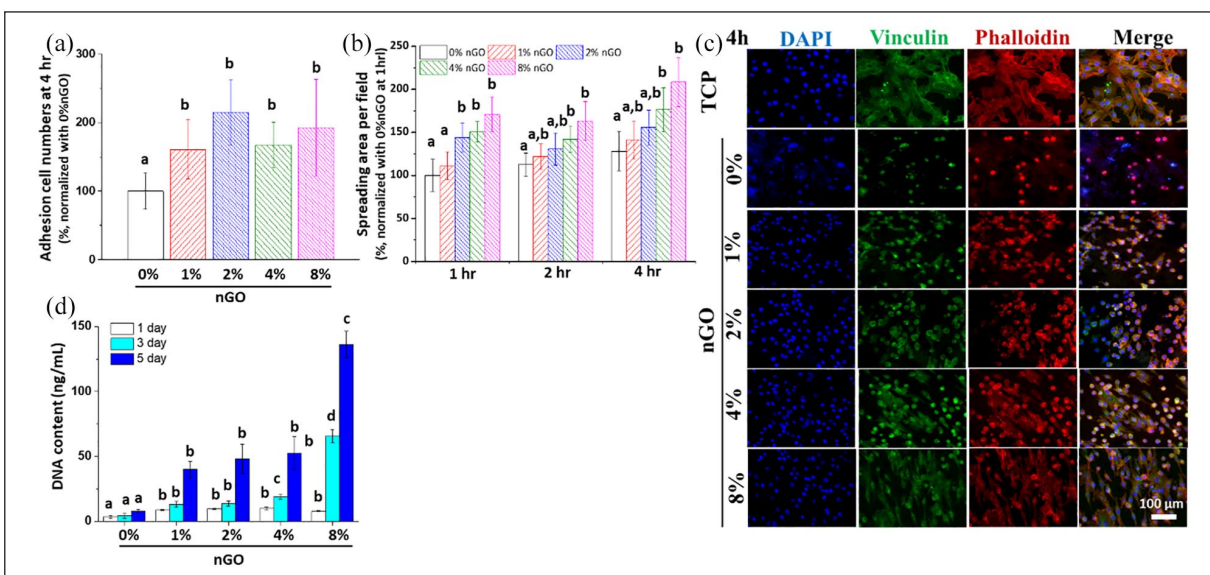

Figure 3. Initial cell adhesion and proliferation of C2C12 to PU-nGO nanofibers. (a) Initial cell numbers of adherent C2C12 on nanofibers and (b) cell spreading area per field at 4 h incubation. PU-nGO nanofibers showed elevated adhesion tendency compared to PU nanofiber and also showed improved spreading capacity along with nGO contents. (c) Vinculin and actin immunocytochemistry at 4 h. Fluorescence intensity increased along with the nGO contents, indicating that cells are more attached and spread to the membrane with higher nGO contents. (d) DNA contents from adherent cells to identify cell proliferation. The 8% PU-nGO showed the highest proliferation capacity. Different letters indicating significant differences among them at the same incubation time condition ($p < 0.05$, $n = 5$).
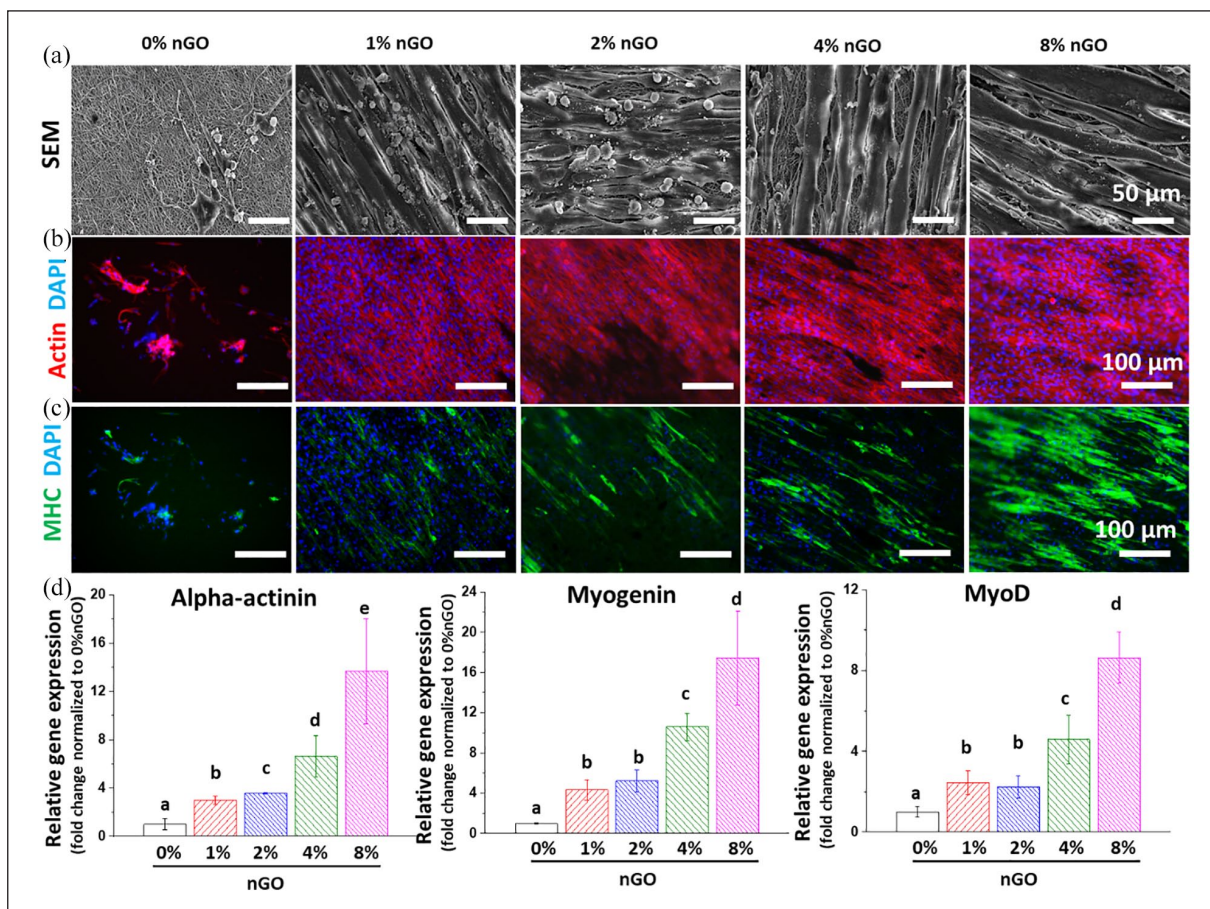
Figure 4. Myogenic differentiation on PU-nGO nanofibers. After 3 days of differentiation on PU-nGO nanofiber, (a) SEM, immunocytochemistry with (b) actin filament and (c) myosin heavy chain (MHC) images were taken. Spread C2C12 cells with thick fibers were observed on PU-nGO by SEM. MHC expression, as well as actin expression, were highly upregulated in 8% PU-nGO compared to others. The 8% PU-nGO nanofibrous membrane showed the most myogenic potential with C2C12 cells. (d) Myogenic gene expression results (alpha-actinin, myogenin, and MyoD). The up-regulations of myogenic gene expression were identified according to the increase of nGO amount in PU nanofibers. The 8% PU-nGO nanofibrous membrane up-regulated myogenic gene expression the most. Different letters indicating significant differences among them ($p < 0.05$, $n = 4$).

greatest proliferative capacity at day 5 compared to others (Figure 3(d)).

Myogenic differentiation capacity of PU or PU-nGO nanofibrous membrane

The myogenic differentiation capacity of PU or PU-nGO nanofiber is determined with C2C12 cells under differentiation conditions (Figure 4). The SEM images and the fluorescent microscopic image showed the distinct striae-like myotubular structure and well-arranged actin filaments in the PU-nGO nanofibrous membrane (Figure 4(a) and (b)). Furthermore, immunocytochemistry data with myosin heavy chain (MHC) showed increased MHC expression tendency in aligned myotubular shape with increasing nGO content: 0% < 1% < 2% ~ 4% < 8% PU-nGO (Figure 4(c)). These myotubes are the structure which the differentiated cells accumulate and construct, and they highly expressed MHC. Consistently, the RT-PCR data revealed

that mRNA expression levels of myogenic markers such as myogenin (MyoG), alpha-actinin, and MyoD are up-regulated in the proportional order to nGO contents: 0% < 1% ~ 2% < 4% < 8% PU-nGO (Figure 4(d)). These results are due to the improved cell adhesion capacity[43,44] invested by ECM-mimicking nanofibrous morphology of PU-nGO matrix. The cells seeded on the elastomer could be mechanically stretched to experience cyclic strain which can enhance myogenic potential.[45] The myogenic differentiation capacity of PU-nGO nanofiber under dynamic tensional stimuli is also validated with C2C12 cells (Figure 5). The dynamic force condision is optimized based on the alpha-actinin expression of the cells (Supplementary Figure 3). Compared to 8% PU-nGO membrane without tension stimulus, 8% PU-nGO membrane with tension stimuli elevated myogenic gene expression, MHC protein expression, and aligned myotubular formation (Figure 5). Our data suggest that an 8% PU-nGO nanofibrous membrane enhanced myogenic gene expression at both mRNA and protein
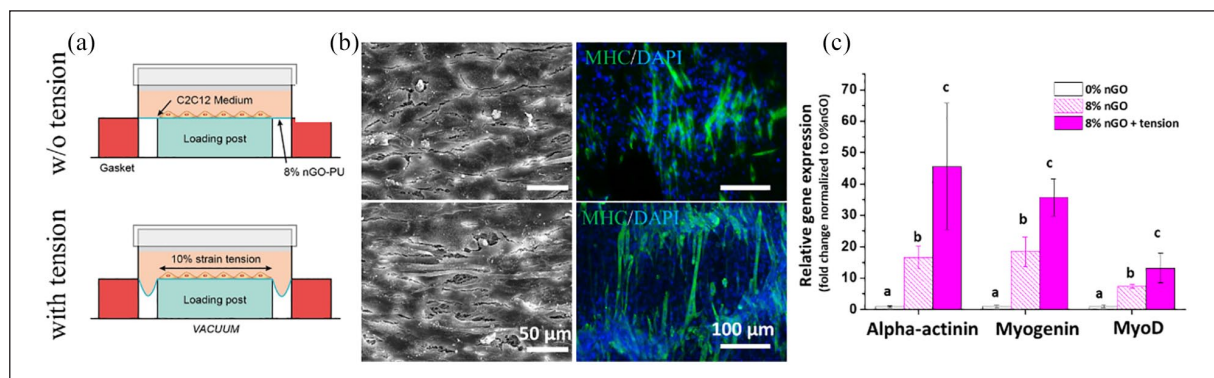
Figure 5. PU-nGO nanofiber synergizes with dynamic mechanical tension in myogenic differentiation. After 3 days of differentiation on 8% PU-nGO nanofiber under dynamic tension force using Flexcell machine (10% strain, 0.5 Hz, 1 h/day), (a) SEM, (b) immunocytochemistry of myosin heavy chain (MHC) images were taken. Fully covered C2C12 cells on 8% PU-nGO nanocomposite were observed by SEM. MHC expression and aligned myotubular formation were highly up-regulated in 8% PU-nGO under dynamic tension compared to static incubation. Dynamic tension and nGO worked in synergy to enhance myogenesis of C2C12 cells. (c) Myogenic gene expression results (alpha-actinin, myogenin, and MyoD). Dynamic tension enhanced myogenic gene expression synergistically with nGO. Different letters indicating significant differences among them ($p < 0.05$, $n = 4$).

levels, even in the dynamic force conditions, implying that the PU-nGO nanofiber as a potential matrix for skeletal muscle engineering.

Conclusion

Here, we developed highly flexible nanocomposite nanofibrous PU-nGO scaffolds that resemble the morphology of natural ECM. The incorporation of nGO to PU improved several mechanical properties such as hydrophilicity, elasticity, and stress relaxation capacity. The PU-nGO nanofibrous membrane enhanced the initial adhesion, spreading, and proliferation of C2C12 cells while presenting little cytotoxicity. Furthermore, these nanofibrous matrices up-regulated myogenic mRNA expression levels and MHC expression. Even under the dynamic tensional force, which is frequently generated by the natural muscle tissue, PU-nGO nanofibers elevated myogenic markers at both mRNA and protein levels, and advanced the aligned myotubular formation. This study suggests PU-nGO nanofibers as a potential matrix for future skeletal muscle engineering.

Author's note

Ahmed El-Fiqi is also affiliated with Glass Research Department, National Research Centre, Cairo, Egypt.

Declaration of conflicting interests

The author(s) declared no potential conflicts of interest with respect to the research, authorship, and/or publication of this article.

Funding

ORCID iDs

Seung Bin Jo [iD] https://orcid.org/0000-0002-9929-8235
Hae-Won Kim [iD] https://orcid.org/0000-0001-6400-6100

Supplemental material

Supplemental material for this article is available online.

References

1. Torii R, Velliou RI, Hodgson D, et al. Modelling multi-scale cell-tissue interaction of tissue-engineered muscle constructs. *J Tissue Eng* 2018; 9: 2041731418787141.
2. Chen J, Dong R, Ge J, et al. Biocompatible, biodegradable, and electroactive polyurethane-urea elastomers with tunable hydrophilicity for skeletal muscle tissue engineering. *ACS Appl Mater Interfaces* 2015; 7(51): 28273–28285.
3. Webb AR, Yang J and Ameer GA. Biodegradable polyester elastomers in tissue engineering. *Expert Opin Biol Ther* 2004; 4(6): 801–812
4. Konow N and Roberts TJ. The series elastic shock absorber: tendon elasticity modulates energy dissipation by muscle during burst deceleration. *Proc Biol Sci* 2015; 282(1804): 20142800.
5. Serrano MC, Chung EJ and Ameer GA. Advances and applications of biodegradable elastomers in regenerative medicine. *Adv Funct Mater* 2010; 20(2): 192–208.
6. Bat E, Zhang Z, Feijen J, et al. Biodegradable elastomers for biomedical applications and regenerative medicine. *Regen Med* 2014; 9(3): 385–398.
7. Marelli B, Alessandrino A, Fare S, et al. Compliant electro-spun silk fibroin tubes for small vessel bypass grafting. *Acta Biomater* 2010; 6(10): 4019–4026.

8.   Jiang T, Carbone EJ, Lo KWH, et al. Electrospinning of polymer nanofibers for tissue regeneration. *Prog Polym Sci* 2015; 46: 1–24.

9.   Lee JH and Kim HW. Emerging properties of hydrogels in tissue engineering. *J Tissue Eng* 2018; 9: 2041731418768285.

10. Christenson EM, Anseth KS, van den Beucken JJ, et al. Nanobiomaterial applications in orthopedics. *J Orthop Res* 2007; 25(1): 11–22.

11. Dashnyam K, Lee JH, Mandakhbayar N, et al. Intra-articular biomaterials-assisted delivery to treat temporomandibular joint disorders. *J Tissue Eng* 2018; 9: 2041731418776514.

12. Divakarla SK, Yamaguchi S, Kokubo T, et al. Improved bioactivity of GUMMETAL®, Ti59Nb36Ta2Zr3O0.3, via formation of nanostructured surfaces. *J Tissue Eng* 2018; 9: 2041731418774178.

13. Damiati L, Eales MG, Nobbs AH, et al. Impact of surface topography and coating on osteogenesis and bacterial attachment on titanium implants. *J Tissue Eng* 2018; 9: 2041731418790694.

14. Levin A, Sharma V, Hook L, et al. The importance of factorial design in tissue engineering and biomaterials science: optimisation of cell seeding efficiency on dermal scaffolds as a case study. *J Tissue Eng* 2018; 9: 2041731418781696.

15. Aviss KJ, Gough JE and Downes S. Aligned electrospun polymer fibres for skeletal muscle regeneration. *Eur Cell Mater* 2010; 19: 193–204.

16. Severt SY, Maxwell SL, Bontrager JS, et al. Mimicking muscle fiber structure and function through electromechanical actuation of electrospun silk fiber bundles. *J Mater Chem B* 2017; 5(40): 8105–8114.

17. Chen Q, Liang S and Thouas GA. Elastomeric biomaterials for tissue engineering. *Prog Polym Sci* 2013; 38(3–4): 584–671.

18. Sears NA, Pena-Galea G, Cereceres SN, et al. Hybrid polyurea elastomers with enzymatic degradation and tunable mechanical properties. *J Tissue Eng* 2016; 7: 2041731416679363.

19. Chattopadhyay DK and Raju KVSN. Structural engineering of polyurethane coatings for high performance applications. *Prog Polym Sci* 2007; 32(3): 352–418.

20. Castagna AM, Fragiadakis D, Lee H, et al. The role of hard segment content on the molecular dynamics of poly(tetramethylene oxide)-based polyurethane copolymers. *Macromolecules* 2011; 44(19): 7831–7836.

21. Madbouly SA and Otaigbe JU. Recent advances in synthesis, characterization and rheological properties of polyurethanes and POSS/polyurethane nanocomposites dispersions and films. *Prog Polym Sci* 2009; 34(12): 1283–1332.

22. Mi H-Y, Jing X, Salick MR, et al. Morphology, mechanical properties, and mineralization of rigid thermoplastic polyurethane/hydroxyapatite scaffolds for bone tissue applications: effects of fabrication approaches and hydroxyapatite size. *J Mater Sci* 2013; 49(5): 2324–2337.

23. Zhao J, Han W, Tu M, et al. Preparation and properties of biomimetic porous nanofibrous poly(L-lactide) scaffold with chitosan nanofiber network by a dual thermally induced phase separation technique. *Mater Sci Eng C Mater Biol Appl* 2012; 32(6): 1496–1502.

24. Sharma Y, Tiwari A, Hattori S, et al. Fabrication of conducting electrospun nanofibers scaffold for three-dimensional cells culture. *Int J Biol Macromol* 2012; 51(4): 627–631.

25. Geim AK. Graphene: status and prospects. *Science* 2009; 329(5934): 1530–1534.

26. Allen MJ, Tung VC and Kaner RB. Honeycomb carbon: a review of graphene. *Chem Rev* 2010; 110(1): 132–145.

27. Depan D, Shah J and Misra RDK. Controlled release of drug from folate-decorated and graphene mediated drug delivery system: synthesis, loading efficiency, and drug release response. *Mat Sci Eng C* 2011; 31(7): 1305–1312.

28. Ren T, Li L, Cai X, et al. Engineered polyethylenimine/graphene oxide nanocomposite for nuclear localized gene delivery. *Polym Chem* 2012; 3(9): 2561–2569.

29. Tu Q, Pang L, Chen Y, et al. Effects of surface charges of graphene oxide on neuronal outgrowth and branching. *Analyst* 2014; 139(1): 105–115.

30. Dong X, Shi Y, Huang W, et al. Electrical detection of DNA hybridization with single-base specificity using transistors based on CVD-grown graphene sheets. *Adv Mater* 2010; 22(14): 1649–1653.

31. Liao KH, Lin YS, Macosko CW, et al. Cytotoxicity of graphene oxide and graphene in human erythrocytes and skin fibroblasts. *ACS Appl Mater Interfaces* 2011; 3(7): 2607–2615.

32. Wang K, Ruan J, Song H, et al. Biocompatibility of graphene oxide. *Nanoscale Res Lett* 2011; 6(1): 1–8.

33. Lammel T, Boisseaux P, Fernández-Cruz ML, et al. Internalization and cytotoxicity of graphene oxide and carboxyl graphene nanoplatelets in the human hepatocellular carcinoma cell line Hep G2. *Part Fibre Toxicol* 2013; 10: 27–21.

34. Chang Y, Yang ST, Liu JH, et al. In vitro toxicity evaluation of graphene oxide on A549 cells. *Toxicol Lett* 2011; 200(3): 201–210.

35. Shi Z, Gao X, Ullah MW, et al. Electroconductive natural polymer-based hydrogels. *Biomaterials* 2016; 111: 40–54.

36. Menzies KL and Jones L. The impact of contact angle on the biocompatibility of biomaterials. *Optom Vis Sci* 2010; 87(6): 387–399.

37. Serrels B, Serrels A, Brunton VG, et al. Focal adhesion kinase controls actin assembly via a FERM-mediated interaction with the Arp2/3 complex. *Nat Cell Biol* 2007; 9(9): 1046–1056.

38. Vicente-Manzanares M, Choi CK and Horwitz AR. Integrins in cell migration-the actin connection. *J Cell Sci* 2009; 122(Pt 2): 199–206.

39. Ezzell RM, Goldmann WH, Wang N, et al. Vinculin promotes cell spreading by mechanically coupling integrins to the cytoskeleton. *Exp Cell Res* 1997; 231(1): 14–26.

40. Kim J, Choi KS, Kim Y, et al. Bioactive effects of graphene oxide cell culture substratum on structure and function of human adipose-derived stem cells. *J Biomed Mater Res A* 2013; 101(12): 3520–3530.

41. Li N, Zhang X, Song Q, et al. The promotion of neurite sprouting and outgrowth of mouse hippocampal cells in culture by graphene substrates. *Biomaterials* 2011; 32(35): 9374–9382.

42. Wang X, Li S, Yan C, et al. Fabrication of RGD micro/nanopattern and corresponding study of stem cell differentiation. *Nano Lett* 2015; 15(3): 1457–1467.

43. Dowling JJ, Vreede AP, Kim S, et al. Kindlin-2 is required for myocyte elongation and is essential for myogenesis. *BMC Cell Biol* 2008; 9: 36.

44. Przewozniak M, Czaplicka I, Czerwinska AM, et al. Adhesion proteins-an impact on skeletal myoblast differentiation. *PLoS ONE* 2013; 8(5): e61760.

45. Dugan JM, Cartmell SH and Gough JE. Uniaxial cyclic strain of human adipose-derived mesenchymal stem cells and C2C12 myoblasts in coculture. *J Tissue Eng* 2014; 5: 2041731414530138.